# Influence of yaw misalignment on the propagation of Tidal Turbine wake

Pranav K. Modali, Ashwin Vinod, and Arindam Banerjee

Abstract—A yaw misalignment to the inflow for tidal current turbines are known to result in performance degradation and deflection of the downstream wake. A comprehensive analysis of the wake behavior under yaw is thus essential to provide insights to marine energy developers for optimizing farm layouts. A detailed understanding of wake deflection and propagation by a yawed turbine is crucial, as, with this knowledge, the wake can be steered away from the downstream turbine. Wake path can be ascertained by tracking the center of the wake and is expected to meander both horizontally and vertically. Several methods are used to determine the center of the wake, most common of which are Gaussian-like fit, Center of mass, and mean available specific power. The variability in these definitions acts as a source of uncertainty in evaluating the wake center at downstream locations. In this paper, we aim to discuss the various methods and evaluate the usefulness of each technique based on the fidelity of the data set that is available. To this effect, we will use results from a threedimensional transient computational fluid dynamics analysis for a tidal turbine subjected to 0°, -15° and +15° yaw cases. Change in wake shape was observed for  $\gamma \neq 0^{\circ}$  yaw cases, where the wake adapts an elliptical shape as it propagates downstream. The center of the mass technique is considered to be the best center of wake estimation technique as it takes into account change in wake shape for yawed flows.

Keywords—tidal stream turbine, yaw, wake, center of the wake

#### I. INTRODUCTION

IDAL Stream Turbines (TST) are renewable energy devices that are being increasingly used to harness power from tides, rivers, and streams without requiring any obstruction to the natural flow of water. Study of TSTs in the scientific literature can be broadly classified into two groups. The first group focusses on the energy extracted by the turbine from water and mostly deals with methods for improving the performance of the turbine. The focus of the second group is on the momentum deficit or wake region behind by the turbine and looks at methods to characterize the deficit and high level of turbulence in the wake region. The wake development behind the turbine is of significant interest as it gives information about the flow modification and turbulence, properties that influence the power output of the downstream turbine in a tidal-farm. Turbine wake development and propagation are influenced by various factors that include turbine operating conditions (rotational speed), turbine geometry and external factors

like the fluid inflow direction, ambient turbulence in the flow and site topology [1]. For tidal turbines, it is not uncommon for the incoming flow to be at an angle (hereafter, referred to as *yaw*) to the axis of the turbine. A yawed inflow may result due to wave-current interaction [2], directional changes in (ebb and flow) tides [3], the presence of upstream bluff bodies [4], and due to the interaction of the flow with the turbine support stanchion (pylon) [5].

The wake behavior for a case of a yawed inflow is very different to flows with no yaw. Relatively few studies [6-10] have looked at scenarios involving a yawed incoming flow to the axis of a TST. Maganga et al. [7] conducted an experimental study to quantify the effects of flow characteristics (yaw, velocity gradient) on the performance and loading of the turbine. Baratchi et al. [9] used actuator line method to study the performance and wake of the tidal turbine with both straight and yawed flow (15° yaw), which was supported using blade element actuator disk method by generating a non-rotational wake. Galloway et al. [2,8] conducted blade element momentum analysis and experimental studies to understand the cyclic loading and fatigue effects due to dynamic yaw on the rotor caused by the wave-current interaction. However, their study provided no details on the downstream wake evolution and meandering. Tian et al. [10] conducted a threedimensional transient computational fluid dynamics (CFD) analysis to understand the effects of yaw and turbulence intensity on the performance and downstream wake structure. Tian et al.'s study explored far-field effects and did not provide detailed observation of the near-wake region (x/D≅10) due to yaw. Yaw effects are also prevalent in scenarios where the incoming flow changes direction due to the course of tides. Park et al. [11] conducted a fluidstructure interaction study to understand the blade deformation and stress on the turbine due to yaw. Previous work by our group [6] explored performance modification, wake development, and propagation due to static yaw in TST using three-dimensional steady-state CFD analysis. Increasing the yaw angle led to a drop in turbine performance; the downstream wake was observed to deflect and meander due to the increasing yaw. A center of the mass technique was used to measure the center of the wake and quantify the meandering nature.

Paper # 1456 was submitted to the "Tidal hydrodynamic modeling (THM) track" at EWTEC2019. Financial support for this work came from the U.S. National Science Foundation (Award # 1706358) through the CBET-Fluid Dynamics Program. P. Modali (sum214@lehigh.edu) and A. Vinod (asv312@lehigh.edu) are Ph.D.

students working with Prof. Arindam Banerjee (arb612@lehigh.edu) as a part of Turbulent Flow Design Group in the Department of Mechanical Engineering & Mechanics, Lehigh University, Bethlehem, PA 18015 USA

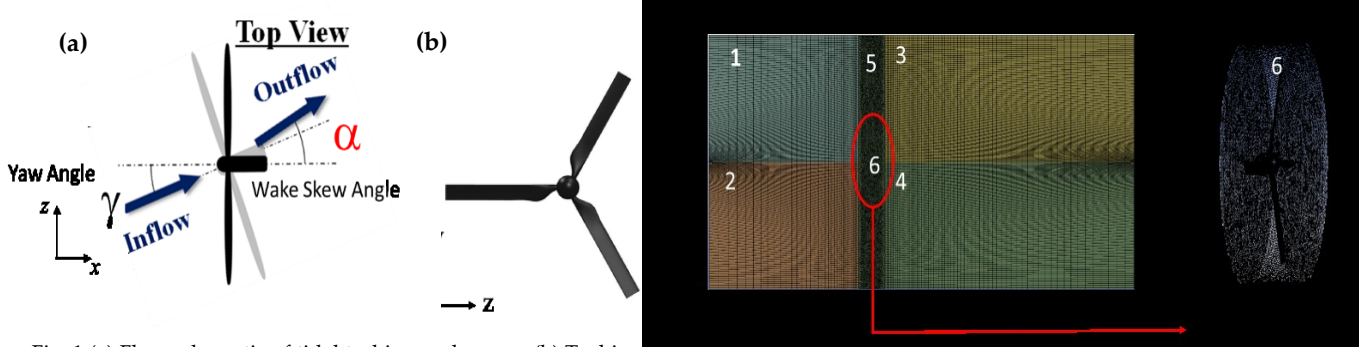


Fig. 1 (a) Flow schematic of tidal turbine under yaw; (b) Turbine used in the current study, (c) wesh used for CFD, (d) limer hard domain. The yaw angle  $(\gamma)$  and the wake skew angle  $(\alpha)$  are shown to illustrate asymmetry in the flow.

Techniques to quantify the wake evolutions and meandering can be found in the wind turbine literature. A brief overview is presented below for the benefit of the readers. Understanding the wake characteristics in wind turbine has been the primary focus of various studies since it plays a prominent role in the performance of a wind farm. Krogstad and Adaramola [12,13], studied the influence of yaw on the near wake characteristics and performance of a wind turbine. The cumulative power output from the farm was observed to increase when the upstream turbine was at yaw to the flow when compared to no yaw case. This was attributed to accelerated wake recovery due to yaw and increased thrust experienced by the downstream turbine. Similar observations were made by Loland [14] who studied wind turbine wake development under yaw and observed that the acceleration in wake recovery is proportional to yaw. The tidal turbines can expect wake behavior similar to this. Several techniques have been introduced in the literature to track the wake meandering. A few notable ones include the methods by Gerbraad et al. [15], Jimenez et al. [16], and Howland et al. [17], etc., which differ based on assumptions made in the derivation of the analytical models and the fidelity of the data-sets used to estimate the wake-center using those models. A recent study by Vollmer et al. [18] compared different techniques under yawed and various ambient wind conditions. The wake deflection was quantified and the lateral thrust components, which are the result of yaw misalignment, were observed and their influence on yaw shape and center of wake described.

In the current study, we use data-sets from three-dimensional transient CFD analysis to quantify the wake development and propagation behind a TST under yawed inflow. The center of the wake is evaluated using a one-and two-dimensional Gaussian fit, the center of mass and mean specific power techniques. The methods are compared to understand the uncertainty in each technique. In addition, wake deflection and change in wake shape due to yaw are evaluated to understand the influence of the cross-stream components on wake propagation.

## II. NUMERICAL METHODOLOGY

#### A. Computational Details

The current simulations were conducted to understand the wake propagation and development around a turbine at a uniform velocity and Reynolds number, using a three-dimensional transient CFD analysis. A detailed description of the CFD setup used in the current simulations can be found elsewhere [6,19]. Turbine wake characteristics were studied for yaw angles ( $\gamma$ , see Fig.1a) of -15° and 15°; these results were compared with a baseline case of 0° yaw. The turbine was operated TSR value of 5 (250 rpm) that corresponds to peak performance for all yaw angles of the turbine [6]. The TST consists of a three-bladed constant chord, untwisted, horizontal axis turbine with a radius (R) of 0.1397 m (see figure 1b). An SG-6043 hydrofoil profile was chosen to maximize the lift coefficient in the operational Reynolds number range of  $10^5 - 10^6$ . The simulation domain was set to mimic an open surface water tunnel with a crosssectional area of 1.2192m  $\times$  1.2192m (8.8R  $\times$  8.8R). Domain size was selected based on the area based blockage, which is discussed in detail in [6]. The current domain was chosen since the blockage ratio is less than 5%. A uniform inlet flow speed ( $U_{\infty}$ ) of 0.73 m/s was chosen. A Reynolds number dependency study was conducted on the same turbine model and reported in a previous study [19]; it was observed that and beyond a velocity (U∞) of 0.73 m/s up to 1.0 m/s, the Reynolds number was observed to have minimum effect on performance for the 1:20 scaled turbine model. A moving mesh technique was employed where the inner fluid domain (see figure 1c), which contains the turbine model, would rotate at a set rotational speed during each time-step until convergence of momentum and continuity equations was reached. The interfaces between the rotating and stationary domains were minimized to eliminate any numerical artefacts in the downstream wake. Based on earlier time step convergence study by our group [19], time step size which corresponds to 2° rotation was chosen to be numerically stable. A mesh

convergence study was also conducted on the basis of the output torque of the TST. Since the primary goal of the current study is to study the wake properties, a wake profile-based convergence study was conducted by varying mesh size from 8 million to 19 million elements; an optimum size of 11 million mesh elements was chosen which had a maximum error, in U velocity component in the wake, of around  $\pm 1\%$ . The mesh quality was maintained based on y+ values, (y<10) for proper prediction of boundary layer separation. The final mesh contains both structured (segments 1-4 in fig. 1(c)) and unstructured mesh (segments 5, 6 in fig. 1(c),(d)) type. The simulations were run until a physical time of 5 seconds in ANSYS-CFX on a system with 256 GB ram and 28 processors which took ~450 hours per simulation.

Reynolds Averaged Navier-Stokes (RANS) equations coupled with the  $\kappa$ - $\omega$  SST (shear stress transport) turbulence model with curvature correction (*CC*) was solved. The mass and momentum conservation equations can be written as

$$\nabla \cdot \vec{U}_r = 0 \tag{1}$$

$$\left[\frac{\partial}{\partial t} \left(\rho \vec{U}_{r,j} + \mathbf{v} \cdot \left(\rho \vec{U}_{r} \otimes \vec{U}_{r,j} + \rho \left(\sum_{r} \vec{U}_{r} + \sum_{r} (\sum_{r} r)\right)\right)\right] = -\nabla p + \nabla \cdot \tau_{f}$$
 (2)

where  $\vec{U}_r = (= \vec{U} - \vec{\Omega} \times \vec{r})$  is the relative velocity viewed from a rotating reference frame,  $\rho(\vec{\Omega} \times \vec{U}_r)$  is Coriolis force,  $\rho(\vec{\Omega} \times \vec{\Omega} \times \vec{r})$  is the centrifugal force,  $\nabla p$  is the pressure gradient across the turbine and  $\tau_f$  is viscous stress tensor. The two equation  $\kappa$ - $\omega$  *SST* model was chosen for its efficiency to predict complex fluid flows under a broad range of adverse pressure gradient conditions [20]. The production term in both the  $\kappa$  and  $\omega$  equations was scaled with a curvature correction term  $f_{\rm rl}$  as:

$$\frac{\partial(\rho k)}{\partial t} + \frac{\partial(\rho u, k)}{\partial x_{i}} = P_{i} f_{i} - \beta^{*} k\omega + \frac{\partial}{\partial x_{i}} \left[ \mu_{d} \frac{\partial k}{\partial x_{i}} \right]$$
(3)

$$\frac{\partial(\rho\omega)}{\partial t} + \frac{\partial(\rho u_{i}\omega)}{\partial x_{i}} = \alpha \rho \frac{P_{k}}{\mu_{i}} f_{r_{1}} - D_{\omega} + Cd_{\omega} + \frac{\partial}{\partial x_{i}} \left[ \mu_{\text{eff}} \frac{\partial\omega}{\partial x_{i}} \right]$$
(4)

where  $\alpha = \alpha_1 F + \alpha_2 (1-F)$ ,  $\alpha_1 = 5/9$ ,  $\alpha_2 = 0.44$ ,  $\beta^* = 0.09$ , are empirical constants of the *SST* model,  $Cd_w$  is the cross-diffusion term in the *SST* model,  $D_w$  is the dissipation term in  $\omega$ -equation [21]. The modified function is defined as:

$$f_{r} = \max \left\{ \min \left( f_{rotation}, 1.25 \right), 0.0 \right\}$$

and,

$$f_{rotation} = \begin{pmatrix} 1 + c \\ r_1 \end{pmatrix} \frac{2r^*}{1+r^*} \begin{bmatrix} 1 - c \\ r_3 \end{bmatrix} \tan^{-1} \begin{pmatrix} c \\ r_2 \end{pmatrix} \begin{bmatrix} c \\ r_2 \end{bmatrix}$$

$$(6)$$

where  $c_{r1}$ (=1),  $c_{r2}$  (=2) and  $c_{r3}$  (=1) were empirical constants [22];  $r^*$  and  $r^*$  were given as:

$$\int_{-\infty}^{\infty} \int_{-\infty}^{\infty} \int_{-\infty}^{\infty$$

$$r^* = \frac{S}{\Omega}; \quad \Omega_{ij} = \frac{1}{2} \left[ \left( \frac{\partial U_i}{\partial x_j} - \frac{\partial U_j}{\partial x_i} \right) + 2\varepsilon_{mji} \Omega_m^{rot} \right]$$
 (8)

where  $S_{ij}$  was the strain rate tensor,  $\Omega_{ij}$  was the rotation tensor,  $\Omega_{m}^{rot}$  was the rate of rotation of the system,  $\omega$  was

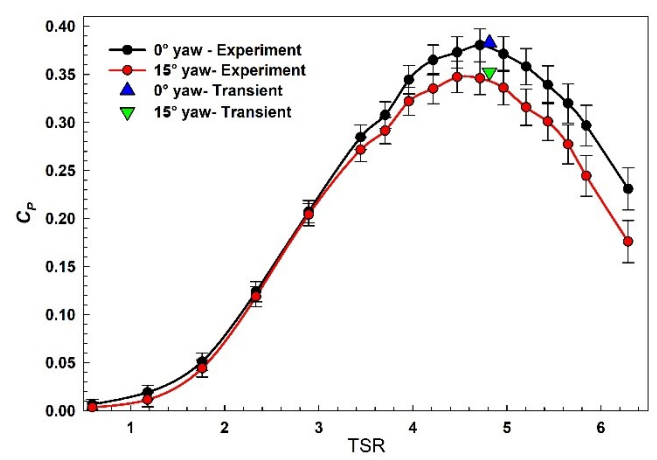


Fig. 2 Comparison of power coefficient ( $C_p$ ) for  $0^\circ$  and -15° yaw cases obtained from transient simulations with  $\kappa$ - $\omega$  SST turbulence model with curvature correction with experimental data.

the turbulent eddy frequency,  $\varepsilon_{ijk}$  is the Levi-Civita operator [23], and variable *D* was defined as:

$$D^2 = \max(S^2, 0.09\omega^2); \quad S^2 = 2S.S. \quad and \quad \Omega^2 = 2\Omega.\Omega.$$
 (9)

## B. Verification and Validation

The numerical technique was validated by comparing the transient simulations with experimental data obtained using an in-house setup [19]. All the experiments reported in this paper were performed in an open surface recirculating water tunnel in our laboratory with a domain cross-sectional size of 0.6096m x 0.6096m. Our tidal turbine model, when operated in the Lehigh water tunnel, led to an (area) blockage of 16.5%. The test setup primarily consists of the turbine blades attached in line to a stepper motor and a thrust-toque sensor, both of which are enclosed in a dry acrylic casing. The stepper motor (Anaheim Automation, Model# 23MSDI) is used for precise control of rotational speeds with a resolution of 1600 steps/rotation, and the thrust-torque sensor is used to measure the thrust (T) and the fluctuating torque ( $\tau$ ) acting on the rotating turbine blades at the rate of 200 samples/second. Both the experimental performance data and data obtained from the CFD simulations were blockage corrected using methods described in Bahaj et al. [24]. A Nortek Vectrino Acoustic Doppler Velocimeter (ADV) was used to measure velocities in the flow field. Wake measurements were made at three downstream locations, 1R, 2R, and 4R from the turbine rotor plane and at the height of 0.9R above the axis of rotation. The obtained time traces were filtered using the phase space thresholding technique [25] to eliminate spikes and ensure data for further analysis. For all wake measurements, the sampling rate and period were maintained at 30 samples/second 40 seconds, respectively.

Primary validation is performed by comparing the performance characteristics from the simulation with the experiments. Non-dimensional parameters that govern the performance of the turbine are the tip speed ratio (TSR), and the power coefficient ( $C_P$ ), which were defined as:

$$TSR = R\Omega/U \tag{10}$$

$$C_{p} = \frac{P_{out}}{\frac{1}{2}\rho AU_{\infty}^{3}} \tag{11}$$

where R was the radius,  $\Omega$  rotor rotational speed in radians/second, U∞ was the freestream velocity, Pout was power output of the turbine (defined as product of torque,  $\tau$ , and angular velocity,  $\omega$ ; P); r was the density of the fluid, A was the swept area of the turbine blades, and T was the thrust force on the rotor plane. Figure 2 presents the performance curve for 0° and -15° yaw cases. It is seen that the Cp results follow a similar response trend; however, have certain quantitative differences dependent on the TSR. The change in the performance between  $0^{\circ}$  and  $-15^{\circ}$ cases at TSR<4 is negligible, beyond which the curves diverge with increasing TSR. Peak performance for both the cases is observed at  $TSR \cong 5$  (250 rpm). The power coefficient obtained from the CFD runs for both the yaw cases predict a Cp value close to the experimentally measured data; however, a slight shift in TSR at this peak Cp values were observed.

In addition to performance metrics, the wake profiles obtained from predicted the simulations were also validated by comparing them to experimental flow measurements for a turbine at -15 $^{\circ}$  yaw using ADV. A normalized velocity deficit ( $U^*$ ) defined as

$$U^* = \frac{U_{\infty} - u(x, y, z)}{U_{\infty}} = \frac{\Delta U(x, y, z)}{U_{\infty}}$$
(12)

where u is the local velocity at any downstream location and  $U_{\infty}$  is the freestream velocity is used for comparison. The wake profile comparisons at three downstream locations, x/R = 1, 2, and 4, are shown in figure 3. At locations closer to the turbine (x/R = 1, 2), both the CFD predictions and experimental measurements are in good agreement in terms of the wake profile shape and width; the velocity deficit profile at these locations was observed to have a top-hat profile, which is typical of a wake that has not undergone diffusion. At x/R = 4, U\* from the CFD simulations can be observed to have a bell-curve shape suggesting increased cross-diffusion of momentum into the wake. The velocity deficit in the wake obtained from the CFD is observed to be lower when compared to experimental data. The wake width obtained from the CFD is observed to be at a higher compared to

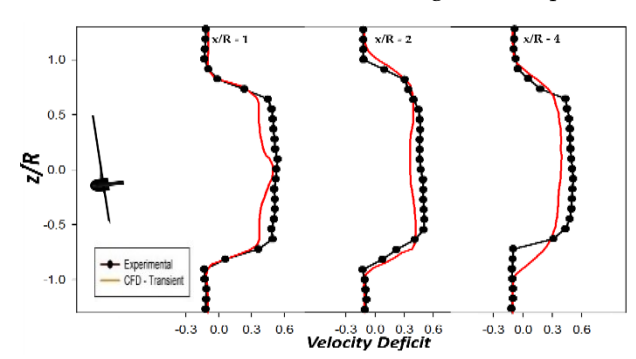


Fig. 3 Comparison of wake deficit behind a turbine (-15° yaw, *TSR* = 5) at three different downstream locations.

experimental data. The deviation in the wake-width from the CFD when compared to experiments is expected as the use of eddy viscosity model is known to cause overly rapid vortex decay that increases diffusivity leading to a quicker recovery of the wake. [22]. Similar trends were observed by Olczak et al. [26] in their RANS simulations.

## C. Techniques to Estimate the Center of Wake

To estimate the center of the wake and trace the wake trajectory, three different methods are compared using our three-dimensional transient CFD data-sets. The methods include (a) Gaussian fitting method, (b) a center of mass technique, and (c) a mean available specific power technique. Each of these techniques is further subdivided into one dimensional (line integral) and two dimensional (area integral) routines to compare estimates from scenarios when centerline velocity measurements are only available with cases where planar (2D) datasets parallel to the rotor plane are available. The one-dimensional routine takes into account only the wake data at the hub height to calculate the center of the wake and ignore the vertical meandering of the wake. The errors are quantified by using a more elaborate two-dimensional technique.

### 1) Gaussian Fit (GF)

In this technique, the position of the wake is calculated by fitting the wake deficit with a Gaussian-like function [27]. For one-dimensional Gaussian fit, the function is defined as [18],

$$f_h(z) = u_a \exp\left(-\left(z - z_c\right)^2 / 2\sigma_z^2\right)$$
 (13)

where  $u_a$  is the amplitude of the wake deficit,  $\sigma_z$  is the width of the wake, and  $z_c$ , the center of the Gaussian fit is considered as the wake-center. Considering the vertical meandering in the wake, a bivariate Gaussian-like fit was proposed by Trujillo et al. [28] and used by Vollmer et al. [18].

$$f_h(z) = u_a \exp \left[ -\frac{1}{2\left(1 - r^2\right)} \left( \frac{\left(z - z_c\right)^2}{\sigma_z^2} - \frac{2\rho\left(y - y_c\right)\left(z - z_c\right)}{\sigma_y\sigma_z} + \frac{\left(y - y_c\right)^2}{\sigma_y^2} \right) \right]$$
(14)

where  $y_c$  and  $z_c$  are the center of the wake co-ordinates which represent the locations on the vertical axis and horizontal axis, respectively, r is a correlation factor between y and z. A perfectly circular wake would have a correlation of zero (i.e., r=0). Earlier studies by our group (for a tidal turbine) [6] and by Howland et al. [17] (for a wind turbine), observed a wake shape close to elliptical or C-shaped with positive correlation, i.e.,  $r\neq 0$  [18]. A least squares approach is used in order to fit both types of Gaussian profiles [18]. The GF technique considers the whole wake region and fits a Gaussian-like curve to estimate the peak location, which is assigned as the center of the wake. For both -15° and +15° yaw cases, large velocity gradients were observed at the wake bounds due to the increased interaction of the wake with the ambient flow. The presence of large gradients and the asymmetric

cross-section of the wake may lead to inaccuracies with the GF technique. However, this technique is the easiest to implement as it does not need any additional processing to the given data.

## 2) Center of Mass (CoM)

In this technique, the wake is considered as a solid body, and the center is estimated as the weighted average of the wake deficit. In estimating the center of wake on the XZ plane at hub height (*y*=0), a one-dimensional center of mass technique is used, based on Howland et al. [17], which is defined as,

$$z'_{c}(x) = \frac{\int z \Delta U(x, y = 0, z) dz}{\int \Delta U(x, y = 0, z) dz}$$
(15)

where  $z_c'$ , is considered as the center of the wake and  $\Delta U$  (=  $U_{\infty} - u(x, y, z)$ ) is the velocity deficit, and u(x, y, z) is the instantaneous velocity. To quantify the meandering in the wake in both horizontal and vertical directions, i.e., along y-axis and z-axis in our coordinate system, a two dimensional center of the mass technique is used, such that,

$$y_c(x) = \frac{\iint y \Delta U(x,y,z) dy dz}{\iint \Delta U(x,y,z) dy dz} \quad ; \quad z_c(x) = \frac{\iint z \Delta U(x,y,z) dy dz}{\iint \Delta U(x,y,z) dy dz} \quad (16)$$

where  $y_c$  and  $z_c$  are the center of wake coordinates. The integration for both one dimensional and two-dimensional fits is performed only over the wake region. The wake bounds are assumed to be within 99% of the free-stream velocity (i.e., a local fluid velocity equal to 99% of free-stream velocity) [6]. The CoM technique, which is more widely used, estimates the center of the wake based on the whole wake as a structure. It calculates the center of the mass considering wake as a body using weighted average and considers that as the center of the wake. This technique takes into account the change in shape, asymmetry of the wake and is sensitive to the large velocity gradients near the wake bounds.

## 3) Mean available specific power (MASP)

Vollmer et al. [18] introduced this method to estimate the center of wake; a hypothetical turbine is assumed at a location downstream of the turbine and mean power that can be captured by that hypothetical turbine is estimated. The location where the least amount of power can be captured is considered as the center of the wake. The formulation is given as [29],

$$f_{AP}(z_{1}) = \frac{1}{2} \int_{z_{1}}^{z_{2}} (u(x, y', z')dz')^{3},$$

$$(z'-z)^{2} \leq (R)^{2}$$

$$z'_{c}(x) = \underset{z_{1}}{\operatorname{argmin}} (f_{AP}(z_{1}))$$
(17)

where u is the instantaneous velocity,  $y_h$  is the hub height (i.e., XZ plane at y=0). This equation is modified in an attempt to relax the constrain of considering only the y locations at hub height and take into account the vertical meandering of the wake. The modified equation acts as a two-dimensional equation, which can be represented as follows,

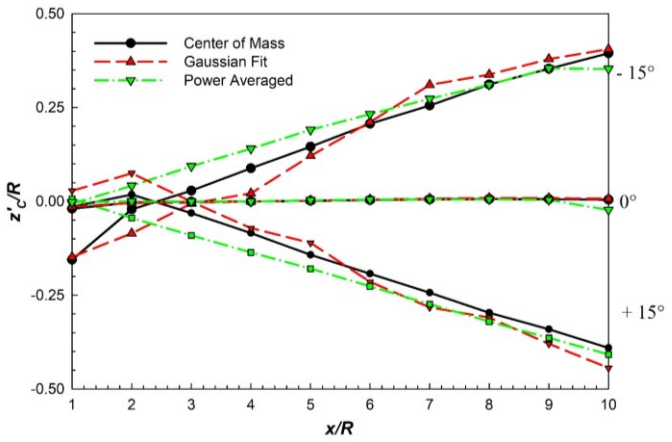


Fig. 4 Wake deflection trajectory calculated using different fit to the wake data (at the hub height,  $y=y_h=0$ ) at different downstream locations. The data resented is obtained using one-dimensional analysis. The numbers on the side represent the yaw angles.

$$\begin{split} f_{AP}(z_1) &= \frac{1}{2} \int_{z_1}^{z_2} \int_{y_1}^{y_2} (u(x, y', z') dy' dz')^3 \\ & (y' - y)^2 + (z' - z)^2 \leq (R)^2 \\ y_c(x) &= \underset{y_1}{\operatorname{argmin}} \left( f_{AP}(y_1) \right); z_c(x) = \underset{z_1}{\operatorname{argmin}} \left( f_{AP}(z_1) \right) \end{split} \tag{18}$$

The MASP technique tracks the wake based on available flow speed (to the rotor) approach. Since the MASP technique does not consider the complete wake, but, just the wake range equivalent to the rotor diameter; it is helpful in tracking the wake and determine its direct impact on a (hypothetical) downstream turbine. The asymmetry of the wake, as well as large velocity gradient at the outer edges, are irrelevant for this technique.

We next discuss a comparison between these three techniques to estimate the center of the wake at different downstream locations ( $1 \le x/R \le 10$ ). The results discussed in section III are averaged over a 1-second duration for t = 4-5 seconds that corresponds to rotation numbers 16-20 of the turbine. Our previous studies [19] have indicated that statistical convergence is attained at ~ $10^{th}$  rotation. For our calculations, the change in the wake (as a structure) was minimal beyond t=4 seconds. It can be assumed that, barring any changes to the inlet or boundary conditions, the wake path is invariant with time.

# III. RESULTS

In this section, the effects of yawed inflow on the wake of a tidal turbine are analyzed. The wake downstream of a horizontal axis turbine is typically divided into two regions. The near wake is a region that is usually within 8-10R (4-5D) downstream of the rotor and is characterized by large swirling motion generated due to rotor [30]. The far wake is a region beyond  $x \ge 5D$  such that the flow can be considered to be independent of the turbine geometry. The computational domain for the simulations reported here extend up to 10R downstream of the rotor plane and analyzed the entire near-wake region. The effect of yaw misalignment for angles of -15° and +15° on the wake

development and propagation was studied and compared to no yaw case.

## D. Estimating the Center of the Wake and Wake Deflection

It is known that the wake generated by the turbine experiences deflection when subjected to yawed inflow [6,10,17]. The different methods discussed in the previous section are used to estimate the center of the wake and quantify the wake deflection. Figure 4 shows the normalized wake deflection on the XZ plane at y = 0 (hub height), for yaw angles of -15°, 0°, and +15° at various downstream locations ( $1 \le x/R \le 10$ ). The center of wake locations is normalized using the turbine radius (R). All three approaches to calculate the center of wake using onedimensional data (i.e., assuming no vertical meandering in the wake (line) is used). The center of the wake for the 0° yaw case was nearly identical at all downstream locations using the three techniques. For both -15° and +15° yaw cases, the GF technique presents the maximum deflection, at locations close to the turbine rotor  $(1 \le x/R \le 5)$ , in the direction away from the actual wake deflection. The center of wake estimation using the CoM and MASP methods show a steady deviation in the direction of yaw for both ±15° yaw cases as the wake propagates downstream. The center of wake estimated by MASP technique is close to the estimates obtained using GF and CoM beyond  $x/R \ge 5$ .

The normalized center of wake coordinates calculated using two-dimensional (planar) data are plotted in a polar plot (see Figure 5) and clearly illustrate the meandering nature of the wake for in the different yaw cases tested. At  $\gamma = 0^{\circ}$ , meandering is restricted to values close to 0.08R. The wake undergoes a slight deviation towards the freesurface and meanders about the vertical (y) axis. As expected, the meandering of the wake is considerably greater at higher yaw angles. For  $\gamma \neq 0^{\circ}$ , wake propagation is categorized into two regions by the authors; the drift region and the post-drift region. In the region close to the turbine rotor, i.e.,  $1 \le x/R \le 6$ , the wake deflects gradually at an angle to the free-stream this segment of the wake is referred to as the drift region. The GF technique predicts the maximum deflection in this region for both yaw cases, whereas, the MASP methods technique estimates the least deflection. The center of the wake can be observed to meander towards and away from the free-surface beyond the drift region. This region is referred to as a post-drift

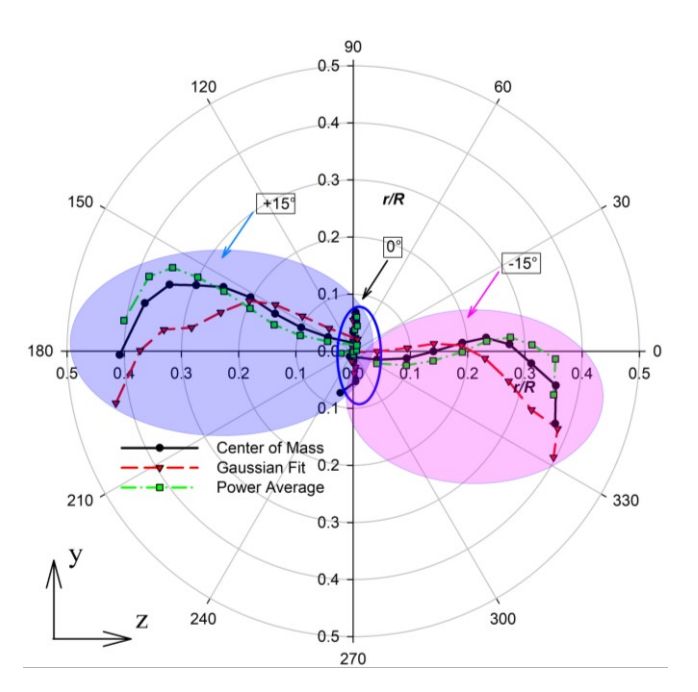
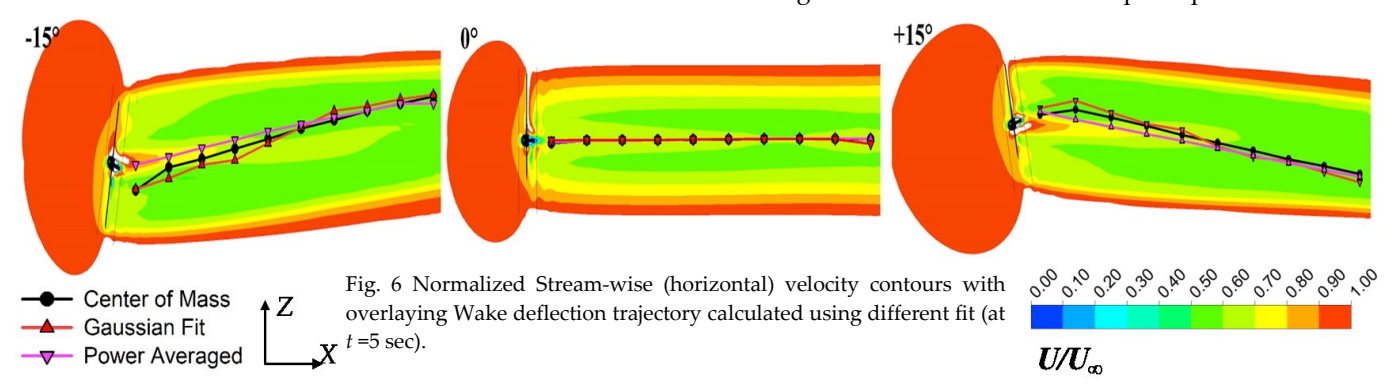


Fig. 5 Wake deflection trajectory calculated using different fit to the wake data using two-dimensional technique at different downstream locations. The region inside the blue enclosure is the scattered center of wake locations for 0° yaw case.

region and was observed to start at  $x/R \ge 5$  for both -15° and +15° yaw cases; the values varied based on the center of wake estimation technique used. The magnitude of deflection based on two-dimensional data was observed to be lower compared to the center of the wake estimates from one-dimensional data. The reasoning is discussed in the next section.

## E. Analysis of Center of Wake Estimation Techniques

Contours of normalized stream-wise velocity ( $U/U_{\infty}$ ) on the XZ plane at y= 0 (hub height), for the different yaw angles, are shown in figure 6. The center of the wake coordinates is overlaid on the contour plots to aid in tracking the wake-center. For all the cases, as the wake propagates downstream, the deficit can be observed to be almost uniformly distributed along the wake region for all downstream locations. For both yaw cases, it was observed that the GF based estimate was closest to the edge, especially in the drift region ( $1 \le x/R \le 6$ ). This suggests that the one-dimensional center of wake calculated based on GF method is not very accurate in this region, as the wake in this region resembles an uneven top-hat profile due to



yaw. The wake center based on CoM technique followed a trend similar to the deficit in the wake.

Figure 7 shows the two-dimensional center of wake locations on a plane parallel to the YZ plane at a downstream location of x/R = 8. The center of the wake estimated using these three different techniques are plotted on the normalized velocity deficit contours in figure 7. The range of the wake region considered for MASP technique is illustrated using a circle (dot-dash line type). For the  $0^{\circ}$  yaw case, the wake can be observed to have a circular shape with a deficit in the wake that moves away from the center (XY) plane. As established before [6], for  $\gamma \neq 0^{\circ}$  cases, change in the shape of the wake can be clearly observed from the figure. The wake was observed to morph into an elliptical shape for both tidal turbines [6]; similar observations have been reported for wind turbine wakes under yaw [17,18].

The source of variation between the one-dimensional estimate and the two-dimensional estimates is the dissimilarity in the proportion of wake cross section analyzed; 2D estimate accounts for the integrated wake cross-section, whereas, 1D estimate accounts for only a segment of the wake assuming it to be an adequate representation of the complete cross-section. Both equations would predict identical center of wake locations when applied on wake with a circular cross-section and a radially (outward) decreasing velocity deficit, similar to 0° yaw case. This, however, is not the case of wake profiles observed in the yawed inflow cases, where, an asymmetric evolution of wake is evident. For  $\gamma \neq 0^{\circ}$ , the transformation in the wake shape moves the maximum velocity deficit zone away from the XZ plane at y=0. Additionally, at hub height, stretching of the wake results in an eventual thinning close to its center, pushing and compressing the local wake deficit. As a result, the 1D estimation, restricted to the y = 0 (XZ) plane, picks up only a portion of the wake deficit that has been pushed in the direction of yaw and

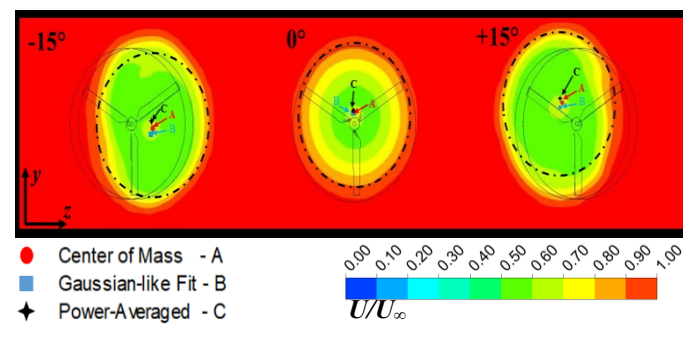


Fig. 7 Normalized velocity contours with overlaying Center of the wake locations calculated using different fit (at t=5 sec) at downstream location of x/R = 8.

misses the bulk of deficit that has moved out of the XZ plane (at y=0). This wake condition becomes more prominent with downstream distance and manifests as more considerable disparities between  $z_c$  and  $z'_c$ . At locations closer to the turbine, the asymmetry is not as dramatic and therefore results in much lower differences between  $z_c$  and  $z'_c$ .

## F. Wake Propagation

It is clear that the wake trajectory is dependent on wake shape. To better understand the origins of the wake deflection and change in the shape of the wake, cross-stream velocity profiles are studied for both -15° and +15° yaw cases and compared with 0° yaw case for reference. Figure 8 presents the normalized velocity contours of U, V, and W velocities which indicate the velocity components in x (downstream direction), y (towards and away from free-surface) and z (direction of the side walls) directions. The red line on the V and W contours represent an outline of the corresponding U velocity. A slowdown of incoming flow can be observed upstream of the turbine for all yaw cases. As discussed earlier, from the U-velocity contour, it can be observed that the deficit in the wake is fairly

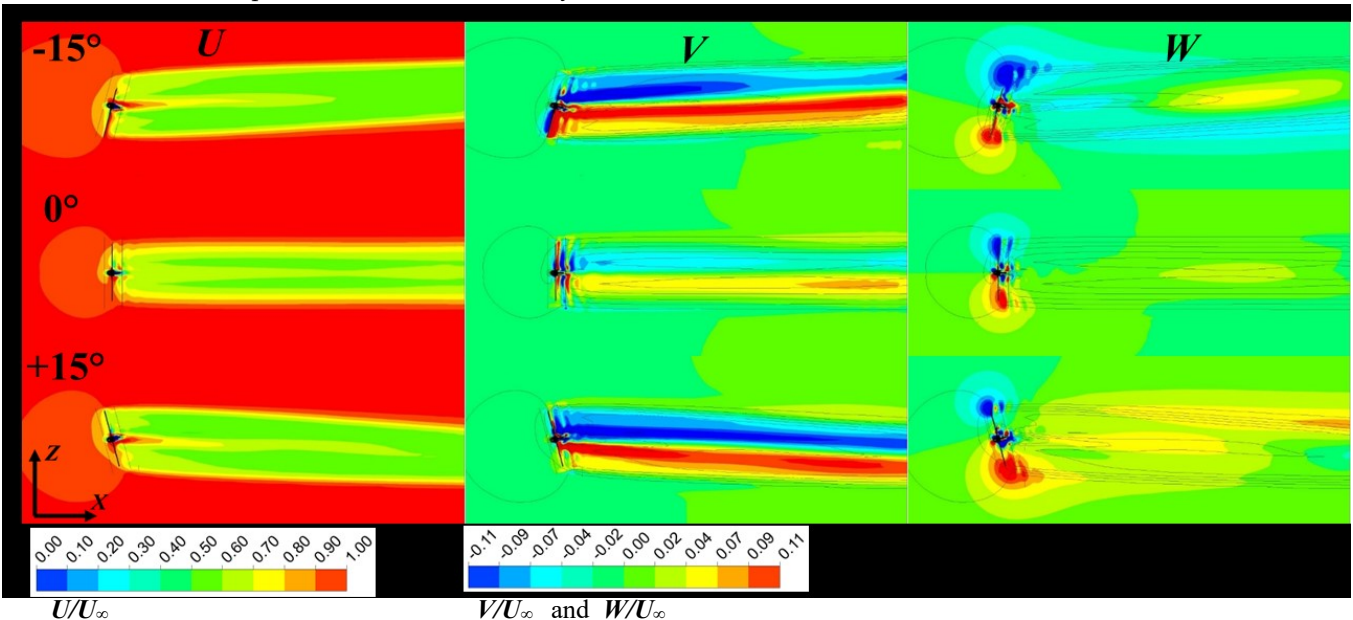


Fig. 8 Normalized U, V and W velocities for  $\gamma = 0^{\circ}$ , -15° and +15° yaw cases at t =5 sec on the XZ plane at y= 0 (hub height). Dark lines on V and W velocity contours represents outline of U velocity. All contours are normalized with the free-stream velocity  $U_{\infty}$ .

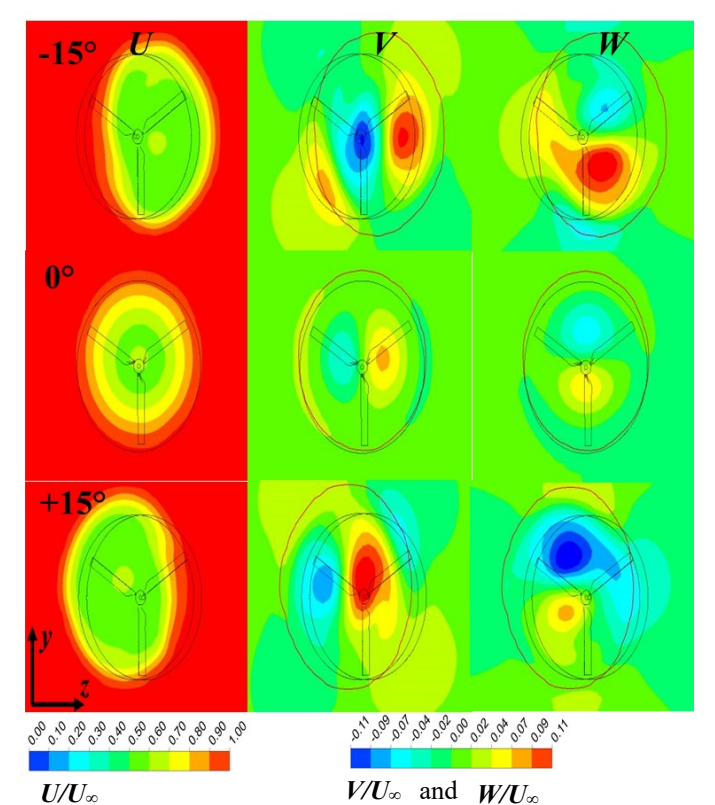


Fig. 9 Normalized U, V and W velocity components for  $\gamma = 0^{\circ}$ , -15° and +15° yaw cases at t = 5 sec and a downstream location of x/R = 8. Dark lines on V and W velocity contour represents outline of U velocity component.

symmetric for the 0° yaw case and wake propagation aligned with the free-stream flow. However, the deficit in the wake, for -15° and +15° yaw cases, is asymmetric but distributed along the wake and is at an angle to the freestream as the wake propagates downstream. The crossstream velocity components play a dominant role in the wake deflection, shape change, and wake recovery. A quick glance at the V velocity reveals that the deficit is fairly symmetric for all yaw cases along the turbine centerline. Stronger *V* velocity values can be observed at the core of the wake, indicating a counterclockwise wake rotation opposite to the turbine rotation. For the cases of +15° and -15° yaw, the downstream evolution of the wake is appreciably more asymmetric; the magnitude of the Vvelocity reduces as the wake moves downstream, suggesting an interruption in wake rotation this was higher for the -15° yaw case. The W velocity shows the deflection in the wake due to yaw. Close to the turbine rotor, strong cross-stream velocity (Z) components can be observed along the wake boundary, resulting in wake deflection noticeable in the  $\pm Z$  directions for  $\mp 15^{\circ}$  yaw cases respectively. The magnitude of the *W* velocity is seen to increase with increasing downstream distance. With downstream travel, the cross-stream components coalesce to influence larger portions of the wake that again aids in subsequent wake recovery.

The cross-stream components play an important role in shaping the wake as it propagates downstream. To understand their influence, velocity profiles of the wake at a downstream location of x/R=8 are plotted in figure 9. The wake (represented by the U velocity) has a nearly

circular shape for zero yaw case. V and W velocities signify the rotation of the wake in a counter-clockwise direction, and the remnant V and W components in the outer rim of the wake suggests wake dissipation. The flow in the outer rim can be observed to rotate in the opposite direction to the wake. At hub height, the velocity distribution is symmetric resulting in a steady (or with minor fluctuations) center of the wake ( $z'_c$ ). The minor uneven distribution of W velocity results in linear fluctuations of the center of the wake ( $z_c$ ) as can be observed in figure 5.

For the yaw cases, the W velocity can be seen to strengthen in the direction of deflection either above or below the hub height (depending on the direction of yaw). The lateral compression in the direction of deflection is observed to result in an elongation in the vertical (y) direction. Regions of steep velocity gradients can be observed for the transverse (W) velocity component in the core region of the wake and is instrumental in pushing the wake in the  $\pm Z$  direction for the  $\mp 15^{\circ}$  yaw cases respectively. Similar tendencies in the wake were observed for wind turbine by Howland et al. [17] and Vollmer et al. [18]. In the wind turbine at yaw, the wake was observed to morph into a C-shaped structure [17] with the wake experiencing a lateral thrust in the direction of deflection close to hub height and in the opposite direction at the top and bottom edges of the wake. Similar behavior of the cross-stream components can be observed in the current study, where the induced cross-stream component at top and bottom of the rotor area stimulates an opposite motion to wake deflection direction, suggesting a possibility for the wake to morph as it propagates further downstream. These opposing cross-stream velocity components, at locations closer to the hub height and near the edges, are responsible for irregular wake displacement at varying heights resulting in an inclined bean or elliptical wake. The combination of cross-stream influences pushes the wake upwards; right for -15° yaw case and left for +15° yaw case. The reader should note that the resulting shape is not symmetric as observed in the actuator disk experiments conducted by Howland et al. [17]. The lower half of the wake for +15° case and the upper half of the wake for -15° case is thicker in the lateral (Z) direction.

## IV. CONCLUSIONS

Transient 3D simulations were performed on a yawed tidal turbine using  $\kappa$ - $\omega$  SST turbulence model with curvature correction. Wake propagation was characterized with the help of normalized velocity contours and by tracking the center of the wake. The primary focus of this study is to understand the uncertainty of the wake deflection estimation based on different techniques available in the literature and data ranges considered for their calculation.

Wake characteristics were studied up to a downstream distance of 10R from the rotor. In an attempt to understand the uncertainty in the wake tracking, three

different techniques used to track the wake were estimated. Based on the comparison, the techniques best suited based on application and the type of inflow can be characterized. The findings from this study can be summarized as follows:

- a. For  $\gamma=0^\circ$  yaw case, due to nearly symmetric wake, the variation between one-dimensional (using a line integral) and two-dimensional (using area integral) definitions are minimal and can be considered negligible. Even the variation between different techniques is nominal; thereby, any technique with one-dimensional data is sufficient to track the wake path.
- b. For  $\gamma \neq 0^{\circ}$  yaw cases, the wake can be observed to be asymmetric; thereby, for an accurate wake tracking, two-dimensional (planar) data provides more accurate estimates. The variation between the center of wake locations estimated by different techniques was discussed. If the wake is being tracked to decide the location of the downstream turbine as in a tidal farm, the MASP technique is suggested since this approach is based on the direct impact of the wake on the energy recovery by the downstream turbine. In this technique, the shape of the wake is irrelevant as it does not consider the whole wake region, and expensive measurement or detailed CFD can be avoided. A Gaussian technique is suited to estimate the center of the wake after the wake reaches self-similarity as the Gaussian-like fit would fit the deficit in a much suitable fashion. Center of the mass technique takes into consideration the whole wake region and also account for the change in the shape of the wake. This technique is well suited to account for the change in wake path as the shape of the wake changes.
- c. The shape change is observed to affect the location of the wake center. The cross-stream components were studied to identify the cause of the shape change in the wake. When the turbine is at yaw, the wake is observed to deflect, causing the cross-stream velocities (V and W) to play an important role in wake development and propagation. The cross-stream components which were observed to instigate the change in shape were also noticed to accelerate the wake dissipation.
- d. The MASP technique does not consider the change in shape, thereby, (indirectly) ignoring the influence of the cross-stream components. While GF technique considers the change in the shape of the wake, it fits a curve to the data, which results in an approximation and is not an exact estimation of the wake center. Based on our studies, the center of mass technique is considered to be the best estimation technique, for yawed flows, as it takes into account the influence of U velocity and cross-stream velocities (as a change in shape) by using the actual data without any fit.

#### **REFERENCES**

- Khan, M., G. Bhuyan, M. Iqbal, and J. Quaicoe, Hydrokinetic energy conversion systems and assessment of horizontal and vertical axis turbines for river and tidal applications: A technology status review. Applied energy, 2009. 86(10): p. 1823-1835.
- Galloway, P.W., L.E. Myers, and A.S. Bahaj, Quantifying wave and yaw effects on a scale tidal stream turbine. Renewable Energy, 2014. 63: p. 297-307.
- Bedard, R., M. Previsic, O. Siddiqui, G. Hagerman, and M. Robinson, Survey and characterization tidal in stream energy conversion (TISEC) devices. EPRI North American Tidal In Stream Power Feasibility Demonstration Project, 2005.
- 4. Chamorro, L., C. Hill, V. Neary, B. Gunawan, R. Arndt, and F. Sotiropoulos, Effects of energetic coherent motions on the power and wake of an axial-flow turbine. Physics of Fluids, 2015. 27(5): p. 055104.
- Frost, C., C.E. Morris, A. Mason-Jones, D.M. O'Doherty, and T. O'Doherty, *The effect of tidal flow directionality on tidal* turbine performance characteristics. Renewable Energy, 2015. 78: p. 609-620.
- Modali, P.K., N. Kolekar, and A. Banerjee, Performance and wake characteristics of a tidal turbine under yaw. International Journal of Marine Energy, 2018. 1(1 (Aug)).
- 7. Maganga, F., G. Germain, J. King, G. Pinon, and E. Rivoalen. Experimental study to determine flow characteristic effects on marine current turbine behaviour. in Proceedings of 8th European Wave and Tidal Energy Conference. 2009. Uppsala, Sweden.
- 8. Galloway, P.W., L.E. Myers, and A.S. Bahaj. Experimental and numerical results of rotor power and thrust of a tidal turbine operating at yaw and in waves. in World Renewable Energy Congress-Sweden; 8-13 May; 2011; Linköping; Sweden. 2011. Linköping University Electronic Press.
- Baratchi, F., T. Jeans, and A. Gerber, Actuator line simulation of a tidal turbine in straight and yawed flows. International Journal of Marine Energy, 2017. 19: p. 235-255.
- Tian, W., J.H. VanZwieten, P. Pyakurel, and Y. Li, Influences of yaw angle and turbulence intensity on the performance of a 20 kW in-stream hydrokinetic turbine. Energy, 2016. 111: p. 104-116.
- 11. Park, S., S. Park, and S.H. Rhee, Influence of blade deformation and yawed inflow on performance of a horizontal axis tidal stream turbine. Renewable Energy, 2016. 92: p. 321-332.
- Krogstad, P.Å. and M.S. Adaramola, Performance and near wake measurements of a model horizontal axis wind turbine. Wind energy, 2012. 15(5): p. 743-756.
- Adaramola, M. and P.-Å. Krogstad, Experimental investigation of wake effects on wind turbine performance.
   Renewable Energy, 2011. 36(8): p. 2078-2086.
- Loland, K.M., Wind turbine in yawed operation. 2011, Institutt for energi-og prosessteknikk.
- Gebraad, P., F. Teeuwisse, J. Van Wingerden, P.A. Fleming,
   Ruben, J. Marden, and L. Pao, Wind plant power optimization through yaw control using a parametric model for wake effects—a CFD simulation study. Wind Energy, 2016.
   19(1): p. 95-114.
- Jiménez, Á., A. Crespo, and E. Migoya, Application of a LES technique to characterize the wake deflection of a wind turbine in yaw. Wind energy, 2010. 13(6): p. 559-572.
- Howland, M.F., J. Bossuyt, L.A. Martínez-Tossas, J. Meyers, and C. Meneveau, Wake structure in actuator disk models of wind turbines in yaw under uniform inflow conditions. Journal of Renewable and Sustainable Energy, 2016. 8(4): p. 043301.
- 18. Vollmer, L., G. Steinfeld, D. Heinemann, and M. Kühn, Estimating the wake deflection downstream of a wind turbine in

- different atmospheric stabilities; an LES study. Wind Energy Science, 2016. 1(2): p. 129-141.
- 19. Kolekar, N. and A. Banerjee, Performance characterization and placement of a marine hydrokinetic turbine in a tidal channel under boundary proximity and blockage effects. Applied Energy, 2015. 148: p. 121-133.
- Spalart, P. and M. Shur, On the sensitization of turbulence models to rotation and curvature. Aerospace Science and Technology, 1997. 1(5): p. 297-302.
- Menter, F.R., M. Kuntz, and R. Langtry, Ten years of industrial experience with the SST turbulence model. Turbulence, heat and mass transfer 4, no. 1 2003: p. 625-632.
- 22. Smirnov, P.E. and F.R. Menter, Sensitization of the SST turbulence model to rotation and curvature by applying the Spalart–Shur correction term. Journal of Turbomachinery, 2009. 131(4): p. 041010.
- Pope, S.B. and S.B. Pope, *Turbulent flows*. 2000: Cambridge university press.
- 24. Bahaj, A., A. Molland, J. Chaplin, and W. Batten, *Power and thrust measurements of marine current turbines under various hydrodynamic flow conditions in a cavitation tunnel and a towing tank.* Renewable energy, 2007. **32**(3): p. 407-426.
- Goring, D.G. and V.I. Nikora, Despiking acoustic Doppler velocimeter data. Journal of hydraulic engineering, 2002. 128(1): p. 117-126.
- 26. Olczak, A., T. Stallard, T. Feng, and P. Stansby, *Comparison of a RANS blade element model for tidal turbine arrays with laboratory scale measurements of wake velocity and rotor thrust.*Journal of Fluids and Structures, 2016. **64**: p. 87-106.
- Parkin, P., R. Holm, and D. Medici. The application of PIV to the wake of a wind turbine in yaw. in Particle Image Velocimetry; Gottingen; 17 September 2001 through 19 September 2001. 2001.
- 28. Trujillo, J.J., F. Bingöl, G.C. Larsen, J. Mann, and M. Kühn, Light detection and ranging measurements of wake dynamics. Part II: two-dimensional scanning. Wind Energy, 2011. **14**(1): p. 61-75.
- 29. Bromm, M., A. Rott, H. Beck, L. Vollmer, G. Steinfeld, and M. Kühn, Field investigation on the influence of yaw misalignment on the propagation of wind turbine wakes. Wind Energy, 2018. **21**(11): p. 1011-1028.
- Myers, L. and A. Bahaj. Near wake properties of horizontal axis marine current turbines. in Proceedings of the 8th European Wave and Tidal Energy Conference. 2009. Uppsala, Sweden.